

# One-dimensional III-V anti-ferroelectirc nanothreads

Zixun Wang<sup>1,2</sup>, Changming Ke<sup>1,3</sup>, Jiawei Huang<sup>1,3</sup>, Shi Liu<sup>1,3\*</sup>

<sup>1</sup>*Institute of Natural Sciences, Westlake Institute for Advanced Study, Hangzhou, Zhejiang 310024, China*

<sup>2</sup>*Key Laboratory of Material Simulation Methods and Software of Ministry of Education & State Key Laboratory of Superhard Materials, College of Physics, Jilin University, Changchun 130012, China*

<sup>3</sup>*Key Laboratory for Quantum Materials of Zhejiang Province, Department of Physics, School of Science, Westlake University, Hangzhou, Zhejiang 310024, China*

## Abstract

One-dimensional (1D) anti-ferroelectrics (AFEs) with multiple stable polar states hold great promise for high-density nonvolatile multistate data storage, the practical application of most AFEs in the information field is hindered by their compatibility issues with silicon-based technology. Furthermore, reported 1D AFEs are still rare, mainly because their polarization is suppressed under nanoscale size. In this study, using density functional theory (DFT), we demonstrate that a family of 1D nanothreads can be obtained by tailoring III-V triatomic layers with good compatibility with silicon-based technology. Through a systematic investigation of these 1D III-V nanothreads, we have identified AlSb as a promising AFE material due to its compatible edge energy and high polarization. The thermodynamic stability and polarization switchability of AFE AlSb have been confirmed through phonon spectrum calculations, *ab initio* molecular dynamics simulations, and ci-NEB methods. These novel materials hold significant promise for memory applications, marking a breakthrough in the field of high-density nonvolatile multistate data storage.

## 1 Introduction

With the emergence of artificial intelligence and big data, the demand for low-power, efficient, and high-density storage of massive data continues to grow. Low-dimensional ferroelectrics (FEs), which possess electrically switchable polarization at atomic level, are considered as promising contenders for fast, efficient, and non-volatile high-density data storage. Recently, a large number of two-dimensional (2D) van der Waals (vdw) FE materials with out-of-plane polarization have been discovered, such as CuInP<sub>2</sub>S<sub>6</sub>[1],  $\alpha$ -In<sub>2</sub>Se<sub>3</sub>[2–7], MoTe<sub>2</sub>[8] and WTe<sub>2</sub>[9]. Storage devices, such as MOS-FET, based on these materials, have also been developed and are now readily available [10, 11]. The prospect of high-density storage solutions based on low-dimensional FE materials has moved a step closer to large-scale practical applications.

Anti-ferroelectrics (AFEs), which is highly correlated with FEs, exhibit electrically switchable antiparallel polarization states without electric field. Specifically, parts of AFEs also exhibit stable parallel polarization ferroelectric states, known as multistability [12–15]. This multistability allows for the expansion of storage bits (expanding 0, 1 to multisates). In theory, an multistate AFE device can store more information compared to FE, attracting significant attention in big data storage field[16, 17]. However, AFE materials are relatively rare, with only a limited number of materials, known to possess AFE properties. Among these materials, only a few exhibit stable multistates. The presence of depolarization fields has a significant impact on reducing the out-of-plane polarization as the size of FE materials decreases. This phenomenon makes the existence of two-dimensional AFEs even more uncommon. Recently, Changming Ke et al. demonstrate with first-principles calculations that III-V triatomic layer, which have depolarization induced 2D tristable anti-ferroelectricity [18]. And these 2D AFEs can be leveraged to create a 2D homojunction field-effect transistor, and easily integrated into the main stream semiconductor industry, opening up new avenues of high-density AFE data storage.

Are there any strategies available to further increase the storage density of 2D AFE nonvolatile devices? A promising and straightforward approach is to employ 1D AFEs, which possess nanosized dimensions in two directions, enabling the development of smaller devices with enhanced data

storage capabilities. Tailoring 2D materials into one-dimensional (1D) structures, such as nanoribbons and nanothreads (NT), has been a prevailing approach for the manufacture of more miniaturized devices in 2D material field. For example, graphene nanoribbons can be rapidly obtained by cutting carbon nanotubes along axis-direction via dynamic magnetic flux template[19].Also, nonmetal  $\text{SiO}_x$  nanoparticles can tailor few-layer graphenes into graphene nanoribbons[20].The h-BN monolayer can be tailored into BN nanoribbons by selectively removing hydrogen along two adjacent grain boundaries in parallel[21]. Typically, the unique characteristics of 1D ferroelectric nanostructures arise from their expanded surface area. Furthermore, as their size and dimensionality decrease, it becomes easier to create single-domain structures, significantly boosting ferroelectric properties[22]. Recently, 1D FEs with radial polarization holds the potential to enable highly compact FE-based electronic devices, wherein a few unit cells, rather than a domain of unit cells, function as the fundamental unit. The discovery of III-VI ferroelectric nanothreads demonstrate the feasibility of obtaining 1DFENT from 2D ferroelectric materials[23]. III-V materials are considered are the materials has the most mature technology except Silicon in electronic technology. A 1D AFE III-V materials can be used to solve many question, such as the compatbilit.

In this study, we present a novel family of 1D III-V nanothreads that exhibit electrically switchable tristates at the atomic scale size, showing great promise for achieving ultra-high density nonvolatile multistate storage. By tailoring III-V 2D triatomic layers with specified edges and width, a family of 1D III-V materials with an ultrasmall diameter is obtained. Using DFT calculations, we demonstrate the coexist of polar phase with radial polarization ( $P_{ra}$ ) and non-polar phase with antiparallel dipole in these materials. Additionally, all of these III-V nanothread structures exhibit semiconductor characteristics, and their dynamic stability is confirmed through phonon spectrum analysis. We found 1D III-V nanothreads possess a higher polarization than 2D, which can be attributed to the quantum confinement effect. Particularly, AlSb stands out with a relatively high polarization of 1.3 eV $\cdot\text{\AA}$ , comparable to that of other typical one-dimensional ferroelectric materials. Moreover, it showcases a low energy difference between the polar and anti-polar structures, suggesting ease of transition between these phases under an electric field. For these reasons, AlSb has been the primary focus of this research. The finite-temperature stability of AlSb 1D Nanothread is confirmed through *ab initio* molecular dynamics. The switch barrier for polarization, evaluated through NEB analysis, is estimated to be around 0.34 eV and can be substantially diminished under an electric field that is antiparallel to the polarization, thereby confirming the electrical tunability of the polar order. The 1DAFENT with radial polarization offers a versatile platform for designing ultrahigh-density ferroelectric memories and exploring novel states of matter.

## 2 Method

First-principles DFT calculations are conducted using the Vienna ab initio Simulation Package (VASP) [24, 25]. The interaction between core ions and electrons is described using the projector augmented wave (PAW) method [26]. The PBEsol functional is chosen for the exchange-correlation functional [27]. To model free-standing 1D nanoribbons, vacuum layers along the x and z axes are set to a minimum of 15 Å. During structural optimization, the dipole correction method [28] is applied along the radial direction.

The lattice constant along the axial direction (y-axis) is determined. We employ an energy cutoff of 600 eV, a 1x8x1 Monkhorst-Pack k-point mesh, and an energy convergence threshold of  $10^{-7}$  eV for electronic self-consistent calculations. The finite-temperature structural stability is assessed through AIMD simulations using VASP. These simulations are performed within a 1x2x1 supercell, employing G-point sampling, an energy cutoff of 400 eV, and a convergence criterion of  $10^{-6}$  eV in energy. Temperature control is realized using the Nose-Hoover thermostat [29], with an equilibrium trajectory of 40 ps yielding the averaged structure. The phonon spectrum is computed using the frozen phonon approach as implemented in Phonopy [30] in conjunction with VASP. The NEB method is also employed to determine the energy barrier of polarization reversal. The pertinent input and output files are available in a publicly accessible repository.

### 3 Results and discussion

#### 3.1 1D structures obtained from different edges and widths.

Triatomic layers (3L) of III-V compounds (III = Al, Ga, In; V = P, As, Sb) is predicted to support 2D anti-ferroelectricity with tristable polar states[18], which possess two electrically switchable polar states and a stable anti-polar states with similar energy level. Fig. 1(a) illustrates the configuration of 2D FEs for 3L III-V materials derived from bulk wurtzite structures. The V atoms in the central layer still exhibit displacement along the z-axis away from the center, while the polarity of the surface layer is eliminated due to surface reconstruction. This displacement is responsible for generating the out-of-plane polarization ( $P_{OP}$ ), with the parallel and antiparallel orientations representing the polar and anti polar phases, as shown in Fig. 1(a), respectively. The top view of 2D III-V 3L highlights a hexagonal arrangement present within each layer of the 3L 2D III-V materials. Consequently, it is possible to achieve 1D structures in both the zigzag and armchair directions[31]. Upon comparing the two directions in detail, we observed that the armchair structures are consistently more stable than the zigzag structures. This stability can be attributed to the armchair structures having fewer dangling bonds [see Sect.I in Supporting Information]. Therefore, the armchair structure is considered to be more experimentally accessible and synthesizable as a 1D III-V material. In the following context, all cutting is performed along the armchair direction.

As the width of 2D materials decreases, the nanoconfinement effect becomes more pronounced, resulting in a decrease in material stability [32–34]. In Fig. 1(b), it can be observed that the cutting energy ( $\Delta E_{cut} = (E_{1D} - E_{2D})/L_{edge}$ , where  $L_{edge}$  represents the length of the materials) generally tends to increase as the width decreases, regardless of whether the structures have even or odd widths.  $\omega_1$  and  $\omega_2$  are the narrowest odd- and even-width structures, respectively. However, our calculations indicate that the  $\omega_1$  structure is unstable SI Sect.III (phono spectrum of  $\omega_1$ ). The inset of Fig. 1(b) showcases the structures along the axial direction of the two narrowest and stable structures, namely  $\omega_2$  and  $\omega_3$ . Among these structures,  $\omega_2$  emerges as the smallest and stable structure, characterized by a single dipole in the width direction. It exhibits a genuine 1D polar order, thus earning the designation of a 1D III-V polar nanothread. As shown in Fig. 1 (c), one unit cell (u.c.) of the 1D III-V polar nanothread consists of two dipoles, exhibit a net polarization along the radial direction ( $P_{ra}$ ). Corresponding to it, two types of antipolar structures can be constructed, as depicted in Fig. 1 (c): one with antiparallel dipoles within a single u.c. (1UCAP), and the other with an antiparallel dipole spanning two u.c. (2UCAP), similar to commonly observed AFEs. We compared the energy of these two types of antipolar structures and found that the 2UCAP structure always has lower energies, as shown in Fig 1 (d). In some cases, it even equals the energy of the polar phase, facilitating the reversible transition between them. Therefore, the 2UCAP structure is considered as the antipolar ground state of III-V nanothreads. In the following context, the term "1D antipolar phase" specifically refers to the armchair 2UCAP-type  $\omega_2$  structures.

#### 3.2 Nanoconfinement effect on 1D III-V polar nanothreads

As the width decreases, the nanoconfinement effect becomes stronger, resulting in significant changes in the fundamental properties of materials due to the size effect [35–38]. In the context of 2D FEs, the polarization is consistently suppressed by the depolarization field at the atomic size scale, leading to smaller polarization compared to bulk materials[39]. Does this phenomenon also apply to 1D FEs? Interestingly, there are notable distinctions between 2D and 1D FEs, as shown in Fig 2 (a).  $P_{ra}$  of 1D III-V nanothreads range from  $0.13 e \cdot \text{\AA}$  to  $0.26 e \cdot \text{\AA}$  per polar atom, which is 1 to 2 times higher than that of corresponding 2D layers. This indicates that the reduction in dimensions enhances the polarization of materials, which is contrary to the trend observed in 2D polar materials. Additionally, the decrease in width also significantly increases the band gap. In 2D layers with  $P_{OP}$ , the band bending between the  $P^+$  surface and  $P^-$  surface, caused by the depolarization field effect, leads to a significant reduction in the bandgap compared to bulk crystals. But in 1D, nanoconfinement becomes predominant, the molecular orbitals become more localized, resulting in narrower bands and wider band gaps[40–42]. As shown in Fig. 2(b), due to the quantum effect, the width of 2D III-V compounds has a substantial influence on the band gap. Additionally, as the radius of V atoms increases, the electronic negativity decreases, resulting in an increase in metallicity. Consequently, the polarization and band gap continuously decrease with the increasing radius of V compounds, as shown in Fig. 2.

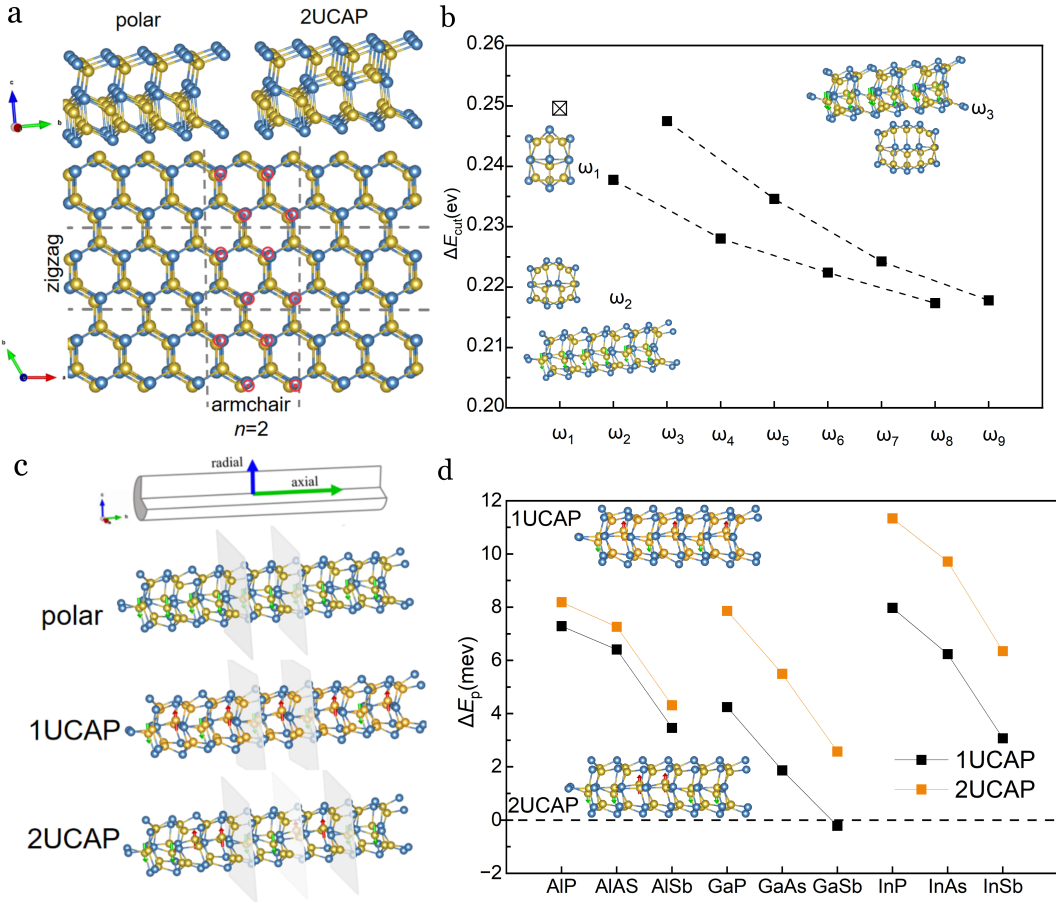


Figure 1: Structural evolution from 2D to 1D . (a) FE and AFE structures of 3L III-V monolayer. The III and V atoms are represented by blue and yellow, respectively. (b)  $E_{\text{cut}}$ , defined as  $\Delta E_{\text{cut}} = (E_{1D} - E_{2D})/L_{\text{edge}}$ , depends on width of low-dimensional III-V materials. (c) Polar and antipolar configuration of armchair  $\omega_2$  (d) Energy difference ( $\Delta E_{\text{AP}}$ ) between the 1D III-V antipolar phase and the polar phase.

For different V atoms, under the influence of nano confinement effect, the band gap of 2D, which ranges from 0-0.3 eV, increases to 0.4-1.6 eV in 1D, greatly expanding the potential applications of III-V based compounds. Due to the stronger metallicity of larger radius V atoms, the valence bond strength is reduced, as shown in Fig. 2 (c). Among the III-V materials, those containing Sb exhibit the smallest  $E_{\text{cut}}$ , comparable to that of graphite nanowire. This suggests that constructing 1D III-V antimonide is more feasible and will be the main focus of Section 3.4.

### 3.3 Phonon stability

We now initiate the estimation of structural stability in 1D III-V polar and antipolar phase by computing phonon spectra following the established protocol for stability analysis in computationally designed materials[43]. A dynamically stable material is characterized by its position at a local energy minimum on the potential energy surface, ensuring that all phonon frequencies are positive. The inherent 1D nature of the system introduces a technical challenge: acoustic phonon modes tend to exhibit low frequencies (close to zero), thus complicating the precise determination of the phonon spectrum numerically. To address this, we employ an exceedingly stringent convergence threshold of 0.01 eV/Å, resulting in the phonon spectra of 1D polar and antipolar 1D III-V nanowires being obtained (Fig. 3). Remarkably, all of these structures exhibit marginal stability, with their lowest frequency falling below  $-2 \text{ cm}^{-1}$ , confirming their dynamic stability at 0K.

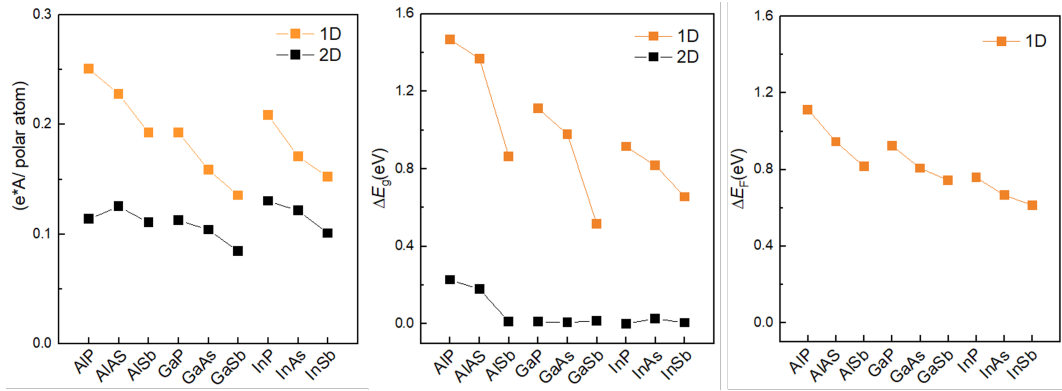


Figure 2: Polarization promotion (a), giant band gap changes (b), and  $\Delta E_{cut}$  (c) of 1D III-V nanothreads.

### 3.4 Tristable 1D AlSb anti-ferroelectrc nanothread

In this section, we will thoroughly discuss the anti-ferroelectricity in 1D III-V nanothread, with a specific focus on 1D AlSb. This material stands out as one of the highest-performing III-V nanothreads, exhibiting switchable tristable polar states, comparable polarization, and relatively small  $\Delta E_{cut}$ . As previously mentioned, the phonon spectrum provides valuable insights into the dynamic stability of structures. However, for a more comprehensive understanding, *ab initio* molecular dynamics (AIMD) simulations at finite temperature are considered more reliable as they accurately capture the temperature effects in practical conditions. A 1x2x1 supercell of 1D AlSb is utilized in our AIMD simulations. As shown in Fig 4 (a), even after a long time of 40 ps at 150K, both the polar and antipolar phases remain stable. Notably, the average structure obtained from the latest 10 ps equilibrium trajectory exhibits consistency with the structure optimized using the 0K DFT method. The polarization originating from the off-centering of Al in AlSb remains exist. The distribution resulting from temperature perturbation is shown in Fig. 4 (b), displaying a standard Gaussian distribution. The average displacement is 0.87 Å, indicating a slight reduction to 0.94 Å at 0K, and demonstrating the stability of polarization at finite temperature. 1D materials are typically placed on substrates and can be significant compressed or stretched. The stability of polarization under strained conditions is particularly important for 1D FEs. Therefore, we investigate the polarization evolution under a wide range strains from -5% to +5%, as show in Fig. 4c, with the increase of tensile strain, the polarization also continuously increased. However, at +5% strain, the polarization is 0.40 e \* Å, confirming the stability of polarization under a very severe strained condition. Moreover, the dipole locking phenomenon observed in the 1D AlSb nanothread suggests the presence of an unusual piezoelectric behavior. The relationship between strain and polarization reveals the existence of what is known as the auxetic piezoelectric effect (APE). In this case, stretching the nanothread amplifies the polarization denoted as  $\mathcal{P}_{ra}$ . This stands in stark contrast to conventional piezoelectric materials, where the longitudinal and transverse piezoelectric coefficients have opposing signs. The auxetic piezoelectric effect can be likened to a piezoelectric counterpart of auxetic materials, which are characterized by a negative Poisson's ratio[23].

The switching pathway is investigated using the ci-NEB (climbing nudged elastic band) method, revealing a unique dynamics in which two dipoles with nearest-neighbor distance switch simultaneously, as shown in the transition states depicted in Fig. 4 (d). The switch barrier is approximately 0.38 eV, which is lower than 0.85 eV of  $In_2Se_3$ , a common 2D material[2]. This outcome suggests the potential for switchable polarization under the influence of an external electric field. It is pertinent to note that the NEB calculations are executed while keeping the lattice constants fixed to the ground-state values of the antipolar phase. Generally, when the lattice constants are allowed to relax during the search for the transition state, the identified switching barrier is expected to be lower than the NEB barrier due to the material's ability to explore a broader spectrum of configurations, potentially uncovering lower-energy pathways. Hence, we contend that the switching barrier computed through NEB represents a conservative estimate of polarization reversibility.

The band structure of the polar and antipolar phases is presented in Fig. 44 (d) and (e), respec-

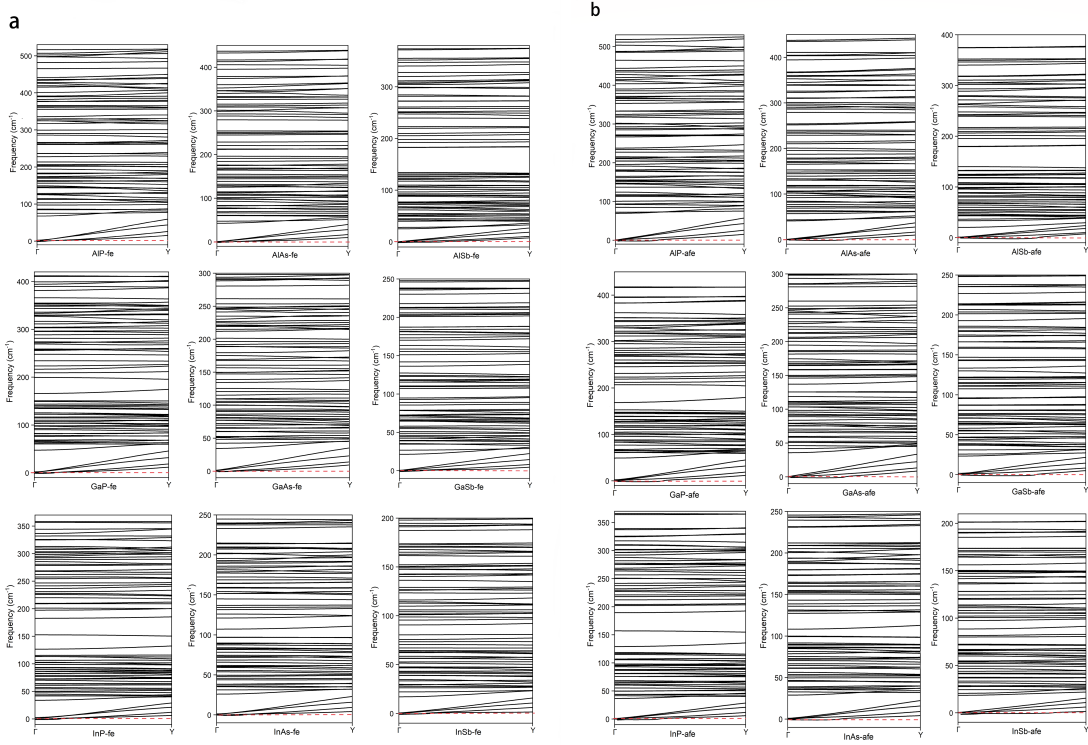


Figure 3: Phonon spectrum of III-V 1D nanothreads. Phonon spectrum of FE (a) and AFE (b) phase.

tively. It reveals that both phases exhibit semiconductor behavior with direct band gaps of both 0.87 eV for the polar and antipolar phases, respectively. Notably, the band structure of polar states in 1D materials is fundamentally distinct from that of 2D FEs. In 2D with  $\mathcal{P}_{\text{OP}}$ , the conduction band minimum (CBM) is typically located at the  $\mathcal{P}+$  surface, while the valence band maximum is found at the  $\mathcal{P}-$  surface, owing to the influence of the depolarization field. However, in the case of AlSb nanothread, the VBM is situated at x atoms on the xx surface, and the CBM is located at the xx surface. Neither of these positions corresponds to the polar atoms or the surface, as depicted in Fig. 4(e). Consequently, after the switching of polarization from the polar to the antipolar phase, the band structure does not exhibit any significant differences. Due to the robust nature of semiconductors, which have fewer carriers available to screen the external field, the polarization in AlSb nanothread can be readily switched by an electric field, as shown in Figure 4(d). With an increase in the field strength from  $-0.3 \text{ V}/\text{\AA}$  to  $0.3 \text{ V}/\text{\AA}$ , the switch barrier decreases from 0.27 eV to 0.49 eV, confirming the electric switchability of AlSb nanothread.

In summary, in light of these findings, we conclude that AlSb nanothread stands as a rare example of a one-dimensional material marked by its tristable and electrically switchable polarization states. Specifically, AlSb nanothread exhibits a 1D tristable antiferroelectricity.

## 4 Conclusion

In conclusion, utilizing first-principles density functional theory calculations, we predict a series of one-dimensional III-V ferroelectric and anti-ferroelectric nanothreads with ultra-small diameters, exhibiting electrically switchable radial polarization. Our study reveals a spontaneous structural transition from nanoribbons to nanothreads as the nanoribbon width decreases. The switchable radial polarization of the  $\omega_2$   $\text{Al}_{12}\text{Sb}_{12}$  nanothread holds the potential to realize highly compact ferroelectric-based electronic devices. The dipole locking feature gives rise to an intriguing 1D auxetic piezoelectric effect that the axial stretching promotes radial polarization. Moreover, the inherently flat electronic bands within the 1D nanothread provide a platform for investigating unique states of matter, such

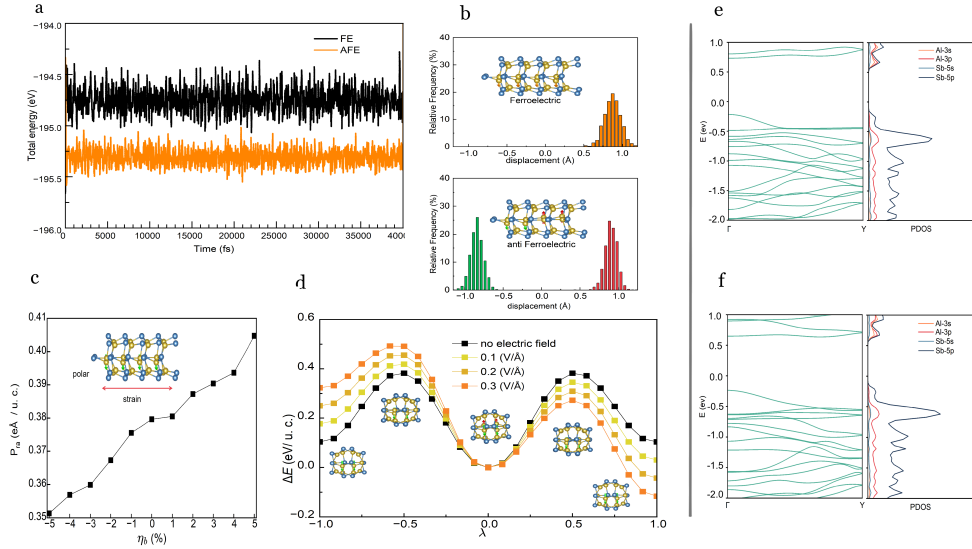


Figure 4: 1D AlSb antiferroelectrics. (a) Energy profile of AIMD at 150K, during 40 ps. (b) Polarization distribution. (c) Dipole vs. strain along axial direction. (d) Polarization switching pathway under electric field predicted by NEB. Projected band structures and DOS of FE (e) and AFE (f) phase.

as Hund's insulator-like semiconductor behavior. Our DFT calculations provide theoretical support for the structural stability of these proposed 1D ferroelectric nanothreads. We anticipate that the proof-of-concept presented in this work will inspire experimental efforts to synthesize this novel family of low-dimensional ferroelectrics.

## 5 Data availability

The data that support the findings of this study are included in this article and are available from the corresponding author upon reasonable request.

## References

- [1] Yue Li, Jun Fu, Xiaoyu Mao, Chen Chen, Heng Liu, Ming Gong, and Hualing Zeng. Enhanced bulk photovoltaic effect in two-dimensional ferroelectric CuInP<sub>2</sub>S<sub>6</sub>. *Nat. Commun.*, 12(1):5896, October 2021.
- [2] Wenjun Ding, Jianbao Zhu, Zhe Wang, Yanfei Gao, Di Xiao, Yi Gu, Zhenyu Zhang, and Wenguang Zhu. Prediction of intrinsic two-dimensional ferroelectrics in In<sub>2</sub>Se<sub>3</sub> and other III<sub>2</sub>-VI<sub>3</sub> van der waals materials. *Nat. Commun.*, 8(1):14956, apr 2017.
- [3] Yu Zhou, Di Wu, Yihan Zhu, Yujin Cho, Qing He, Xiao Yang, Kevin Herrera, Zhaodong Chu, Yu Han, Michael C. Downer, Hailin Peng, and Keji Lai. Out-of-plane piezoelectricity and ferroelectricity in layered α-In<sub>2</sub>Se<sub>3</sub> nanoflakes. *Nano Lett.*, 17(9):5508–5513, August 2017.
- [4] Chaojie Cui, Wei-Jin Hu, Xingxu Yan, Christopher Addiego, Wenpei Gao, Yao Wang, Zhe Wang, Linze Li, Yingchun Cheng, Peng Li, Xixiang Zhang, Husam N. Alshareef, Tom Wu, Wenguang Zhu, Xiaoqing Pan, and Lain-Jong Li. Intercorrelated in-plane and out-of-plane ferroelectricity in ultrathin two-dimensional layered semiconductor In<sub>2</sub>Se<sub>3</sub>. *Nano Lett.*, 18(2):1253–1258, feb 2018.
- [5] Jun Xiao, Hanyu Zhu, Ying Wang, Wei Feng, Yunxia Hu, Arvind Dasgupta, Yimo Han, Yuan Wang, David A. Muller, Lane W. Martin, PingAn Hu, and Xiang Zhang. Intrinsic two-dimensional ferroelectricity with dipole locking. *Phys. Rev. Lett.*, 120:227601, May 2018.

- [6] Sock Mui Poh, Sherman Jun Rong Tan, Han Wang, Peng Song, Irfan H. Abidi, Xiaoxu Zhao, Jiadong Dan, Jingsheng Chen, Zhengtang Luo, Stephen J. Pennycook, Antonio H. Castro Neto, and Kian Ping Loh. Molecular-beam epitaxy of two-dimensional In<sub>2</sub>Se<sub>3</sub> and its giant electroresistance switching in ferroresistive memory junction. *Nano Lett.*, 18(10):6340–6346, September 2018.
- [7] Siyuan Wan, Yue Li, Wei Li, Xiaoyu Mao, Wenguang Zhu, and Hualing Zeng. Room-temperature ferroelectricity and a switchable diode effect in two-dimensional  $\alpha$ -In<sub>2</sub>Se<sub>3</sub> thin layers. *Nanoscale*, 10(31):14885–14892, 2018.
- [8] Shuguo Yuan, Xin Luo, Hung Lit Chan, Chengcheng Xiao, Yawei Dai, Maohai Xie, and Jianhua Hao. Room-temperature ferroelectricity in MoTe<sub>2</sub> down to the atomic monolayer limit. *Nat. Commun.*, 10(1):1175, April 2019.
- [9] Zaiyao Fei, Wenjin Zhao, Tauno A. Palomaki, Bosong Sun, Moira K. Miller, Zhiying Zhao, Jiaqiang Yan, Xiaodong Xu, and David H. Cobden. Ferroelectric switching of a two-dimensional metal. *Nature*, 560(7718):336–339, July 2018.
- [10] Wanying Li, Yimeng Guo, Zhaoping Luo, Shuhao Wu, Bo Han, Weijin Hu, Lu You, Kenji Watanabe, Takashi Taniguchi, Thomas Alava, Jiezhi Chen, Peng Gao, Xiuyan Li, Zhongming Wei, Lin-Wang Wang, Yue-Yang Liu, Chengxin Zhao, Xuepeng Zhan, Zheng Vitto Han, and Hanwen Wang. A gate programmable van der waals metal-ferroelectric-semiconductor vertical heterojunction memory. *Advanced Materials*, 35(5):2208266, 2023.
- [11] Lu Qi, Shuangchen Ruan, and Yu-Jia Zeng. Review on recent developments in 2d ferroelectrics: Theories and applications. *Advanced Materials*, 33(13):2005098, 2021.
- [12] T. Durga Rao, Saket Asthana, and Manish K. Niranjan. Observation of coexistence of ferroelectric and antiferroelectric phases in sc substituted bfeo<sub>3</sub>. *Journal of Alloys and Compounds*, 642:192–199, 2015.
- [13] Guilhermina Ferreira Teixeira, Heitor Secco Seleghini, Wagner Benício Bastos, Natalia Jacomaci, Bojan Stojadinović, Zorana Dohčević-Mitrović, Flavio Colmati, Miguel Angel San-Miguel, Elson Longo, and Maria Aparecida Zaghete. On the coexistence of ferroelectric and antiferroelectric polymorphs in nanbo<sub>3</sub> fibers at room temperature. *J. Mater. Chem. C*, 11:5524–5533, 2023.
- [14] Zimeng Hu, Vladimir Koval, Yajun Yue, Man Zhang, Chenglong Jia, Isaac Abrahams, and Haixue Yan. Structural evolution and coexistence of ferroelectricity and antiferromagnetism in fe, nb co-doped batio<sub>3</sub> ceramics. *Journal of the European Ceramic Society*, 43(6):2460–2468, 2023.
- [15] R. A. Shakhovoy, S. I. Raelevskaya, L. A. Shakhovaya, D. V. Suzdalev, I. P. Raevski, Yu. I. Yuzyuk, A. F. Semenchev, and M. El Marssi. Ferroelectric q and antiferroelectric p phases' coexistence and local phase transitions in oxygen-deficient nanbo<sub>3</sub> single crystal: micro-raman, dielectric and dilatometric studies. *Journal of Raman Spectroscopy*, 43(8):1141–1145, 2012.
- [16] Nava Setter, Dragan Damjanovic, Lukas M. Eng, Glen R. Fox, Spartak Gevorgian, Seungbum Hong, Angus I. Kingon, Hermann Kohlstedt, No yeol Park, G. Brian Stephenson, Igor Stolitchnov, A. K. Taganstev, D. V. Taylor, Tomoaki Yamada, and Stephen K. Streiffer. Ferroelectric thin films: Review of materials, properties, and applications. *Journal of Applied Physics*, 100:051606, 2006.
- [17] M. E. Lines and A. M. Glass. *Principles and Applications of Ferroelectrics and Related Materials*. Oxford University Press, 02 2001.
- [18] Changming Ke, Yihao Hu, and Shi Liu. Depolarization induced iii–v triatomic layers with tristable polarization states. *Nanoscale Horiz.*, 8:616–623, 2023.
- [19] Jinhong Hou, Ruifeng Qi, Yanjing Liang, Yong Cheng, and Qingsong Huang. Tailoring carbon nanotubes quickly into graphene nanoribbons along axis-direction via dynamic magnetic flux template. *Carbon*, 208:338–344, 2023.

- [20] Libo Gao, Wencai Ren, Bilu Liu, Zhong-Shuai Wu, Chuanbin Jiang, and Hui-Ming Cheng. Crystallographic tailoring of graphene by nonmetal siox nanoparticles. *Journal of the American Chemical Society*, 131(39):13934–13936, Oct 2009.
- [21] Jun Yin, Jin Yu, Xuemei Li, Jidong Li, Jianxin Zhou, Zhuhua Zhang, and Wanlin Guo. Large single-crystal hexagonal boron nitride monolayer domains with controlled morphology and straight merging boundaries. *Small*, 11(35):4497–4502, 2015.
- [22] Longyue Liang, Xueliang Kang, Yuanhua Sang, and Hong Liu. One-dimensional ferroelectric nanostructures: Synthesis, properties, and applications. *Advanced Science*, 3(7):1500358, 2016.
- [23] Jiawei Huang, Changming Ke, Wei Zhu, and Shi Liu. One dimensional ferroelectric nanowires with axial and radial polarization. *Nanoscale Horiz.*, 8:1205–1216, 2023.
- [24] G Kresse and Furthmüller J. Efficient iterative schemes for *ab initio* total-energy calculations using a plane-wave basis set. *Phys. Rev. B*, 54(16):11169–11186, 1996.
- [25] G Kresse and Furthmüller J. Efficiency of ab-initio total energy calculations for metals and semiconductors using a plane-wave basis set. *Comput. Mater. Sci.*, 6:15–50, 1996.
- [26] P E Blochl. Projector augmented-wave method. *Phys. Rev. B*, 50:17953–17979, 1994.
- [27] John P. Perdew, Adrienn Ruzsinszky, Gábor I. Csonka, Oleg A. Vydrov, Gustavo E. Scuseria, Lucian A. Constantin, Xiaolan Zhou, and Kieron Burke. Restoring the density-gradient expansion for exchange in solids and surfaces. *Phys. Rev. Lett.*, 100:136406, 2008.
- [28] L. Bengtsson. Dipole correction for surface supercell calculations. *Phys. Rev. B*, 59:12301–12304, 1999.
- [29] Shuichi Nosé. A unified formulation of the constant temperature molecular dynamics methods. *J. Chem. Phys.*, 81(1):511–519, 1984.
- [30] Atsushi Togo and Isao Tanaka. First principles phonon calculations in materials science. *Scr. Mater.*, 108:1–5, 2015.
- [31] K. S. Novoselov. Electric field effect in atomically thin carbon films. *Science*, 306(5696):666–669, oct 2004.
- [32] Yucheng Huang, Chongyi Ling, Zhen Fang, and Sufan Wang. Width- and edge-dependent magnetic properties, electronic structures, and stability of  $\text{SnSe}_{1-x}\text{S}_x$  nanoribbons. *PHYSICA E-LOW-DIMENSIONAL SYSTEMS & NANOSTRUCTURES*, 59:102–106, MAY 2014.
- [33] Traian Dumitrică, Ming Hua, and Boris I. Yakobson. Endohedral silicon nanotubes as thinnest silicide wires. *Phys. Rev. B*, 70:241303, Dec 2004.
- [34] Tim H. Osborn and Amir A. Farajian. Stability of lithiated silicene from first principles. *The Journal of Physical Chemistry C*, 116(43):22916–22920, 2012.
- [35] M. Shaat, U. Javed, and S. Faroughi. Wettability and confinement size effects on stability of water conveying nanotubes. *Scientific Reports*, 10(1):17167, Oct 2020.
- [36] Ryutaro Souda. Nanoconfinement effects of water on hydrophilic and hydrophobic substrates at cryogenic temperatures. *The Journal of Physical Chemistry C*, 116(39):20895–20901, Oct 2012.
- [37] Angela B. Grommet, Moran Feller, and Rafal Klajn. Chemical reactivity under nanoconfinement. *Nature Nanotechnology*, 15(4):256–271, Apr 2020.
- [38] Minjee Seo and Taek Dong Chung. Nanoconfinement effects in electrochemical reactions. *Current Opinion in Electrochemistry*, 13:47–54, 2019. Fundamental and Theoretical Electrochemistry Physical and Nanoelectrochemistry.
- [39] Xin Jin, Yu-Yang Zhang, and Shixuan Du. Recent progress in the theoretical design of two-dimensional ferroelectric materials. *Fundamental Research*, 3(3):322–331, 2023.

- [40] Young-Woo Son, Marvin L. Cohen, and Steven G. Louie. Energy gaps in graphene nanoribbons. *Phys. Rev. Lett.*, 97:216803, Nov 2006.
- [41] Melinda Y. Han, Barbaros Özyilmaz, Yuanbo Zhang, and Philip Kim. Energy band-gap engineering of graphene nanoribbons. *Phys. Rev. Lett.*, 98:206805, May 2007.
- [42] Verónica Barone, Oded Hod, and Gustavo E. Scuseria. Electronic structure and stability of semiconducting graphene nanoribbons. *Nano Letters*, 6(12):2748–2754, Dec 2006.
- [43] H Peelaers, B Partoens, and FM Peeters. Phonon band structure of si nanowires: a stability analysis. *Nano lett.*, 9(1):107–111, 2009.